

## MIT Open Access Articles

*Pressure-Modulated Selective Electrokinetic Trapping for Direct Enrichment, Purification, and Detection of Nucleic Acids in Human Serum*

The MIT Faculty has made this article openly available. **Please share** how this access benefits you. Your story matters.

**As Published:** 10.1021/ACS.ANALCHEM.8B02330

**Publisher:** American Chemical Society (ACS)

**Persistent URL:** <https://hdl.handle.net/1721.1/134740>

**Version:** Author's final manuscript: final author's manuscript post peer review, without publisher's formatting or copy editing

**Terms of Use:** Article is made available in accordance with the publisher's policy and may be subject to US copyright law. Please refer to the publisher's site for terms of use.



# Pressure-Modulated Selective Electrokinetic Trapping for Direct Enrichment, Purification, and Detection of Nucleic Acids in Human Serum

Wei Ouyang,<sup>†,‡,§</sup> Zirui Li,<sup>\*,§</sup> and Jongyoon Han<sup>\*,†,‡,§,||</sup>

<sup>†</sup>Department of Electrical Engineering and Computer Science, Massachusetts Institute of Technology, Cambridge, Massachusetts 02139, United States

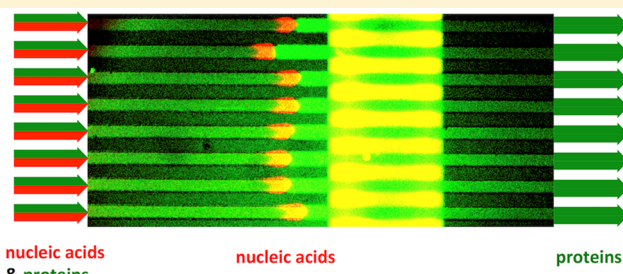
<sup>‡</sup>Research Laboratory of Electronics, Massachusetts Institute of Technology, Cambridge, Massachusetts 02139, United States

<sup>§</sup>Institute of Laser and Optoelectronic Intelligent Manufacturing, College of Mechanical and Electrical Engineering, Wenzhou University, Wenzhou 325035, PR China

<sup>||</sup>Department of Biological Engineering, Massachusetts Institute of Technology, Cambridge, Massachusetts 02139, United States

## Supporting Information

**ABSTRACT:** Micro total-analysis systems ( $\mu$ TAS) have been extensively developed for the detection of nucleic acids (NAs) in resource-limited settings in recent years, yet the sample-preparation steps that interface real-world samples with on-chip analytics remain as the technical bottleneck. We report pressure-modulated selective electrokinetic trapping (PM-SET) for the direct enrichment, purification, and detection of NAs in human serum in one step without involving tedious solid-phase extraction, chemical amplification, and surface-hybridization-based assays. Under appropriately modulated hydrostatic pressures, NAs in human serum were selectively enriched in an electrokinetic concentrator with the majority of background proteins removed, achieving an enrichment factor of >4800 in 15 min. A sequence-specific NA was detected simultaneously during the enrichment process using a complementary morpholino (MO) probe, realizing a limit of detection of 3 pM in 15 min. PM-SET greatly reduces the cost, time, and complexity of sample preparation for NA detection and could be easily interfaced with existing NA-detection devices to achieve true sample-to-answer biomolecular analytics.



The detection of nucleic acids plays a paramount role in genetic analysis, disease diagnosis, food and environment monitoring, and many other research fields.<sup>1–6</sup> In recent years, micro total-analysis systems ( $\mu$ TAS), or lab-on-a-chip devices, have been extensively developed for the detection of NAs, owing to their merits of consuming small amounts of sample; having short turn-around times, high sensitivity, and low cost; and being deployable in resource-limited settings.<sup>7–12</sup> Despite the significant advances in the analytics portion of lab-on-a-chip devices for NA detection, the sample-preparation portion that interfaces real-world samples with on-chip analytics remains underdeveloped, which has surfaced as the limiting factor in the realization of true sample-to-answer systems.<sup>13–20</sup> Currently, the sample-preparation procedures for NA analysis typically include the following. (1) Purification: Solid-phase extraction (SPE) using silica-membrane spin columns, magnetic silica beads, or other capture agents followed by washing and elution with chemicals, which is costly and laborious, requires dedicated equipment and uses chemicals that may inhibit downstream assays. Although miniaturized SPE techniques have been successfully integrated on chips, they typically require specialized and expensive materials and

fabrication processes, use complex structures and protocols for fluid control, and still suffer from compatibility problems with downstream assays.<sup>21–31</sup> (2) Enrichment: The need to detect trace amounts of NAs in real-world samples often necessitates the amplification of NAs before on-chip analytics by polymerase chain reaction (PCR) or other similar techniques. Although on-chip NA amplification techniques have been well developed, there remain considerable limitations for point-of-care applications, such as the requirement of high levels of sample purity, the need for thermal cycling for PCR, complex operating protocols, and others.<sup>32–37</sup> Therefore, in order to achieve true micro “total” analysis systems for NA detection, it is of high priority to develop fully integratable sample-preparation techniques for the purification and enrichment of NAs that overcome the challenges met in SPE and PCR.

Ion-concentration-polarization (ICP)-based electrokinetic trapping (ET) has attracted much attention in the past decade as a viable approach for the rapid concentration of NAs and

Received: May 25, 2018

Accepted: August 29, 2018

Published: August 29, 2018



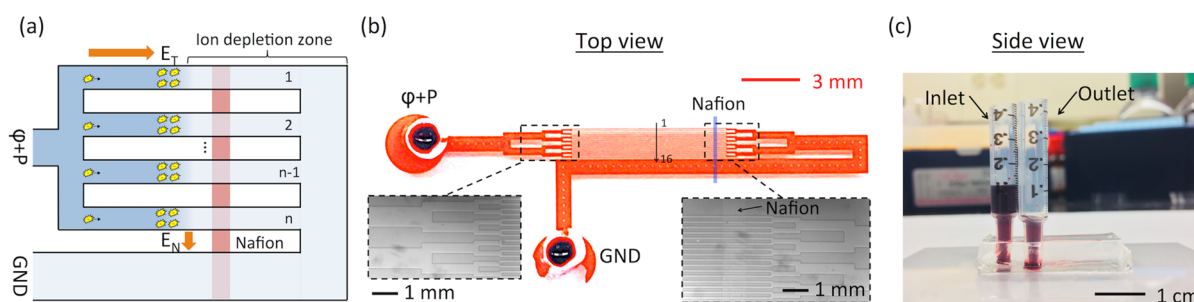


**Figure 1.** Schematic and photos of the device. (a) Schematic of a multiplexed ICP-based ET device. (b) Top-view photo of the device fabricated by PDMS-glass bonding and enlarged views of the device near the splitting and converging channels. (c) Side-view photo of the device.

other biomolecules, with enrichment speeds of  $10^3$ - to  $10^4$ -fold in  $\sim 10$  min and maximum enrichment factors of over  $10^6$  achieved in clean buffers.<sup>38–42</sup> In ICP-based ET, the selective transport of cations through a cation-exchange membrane (CEM) under a DC electric field induces an ion-depletion zone with significantly amplified electric fields in the microchannel, which acts as an electric-force barrier that prevents the passage of negatively charged species. Negatively charged species enter the microchannel with an electroosmotic flow (EOF) under a tangential electric field and subsequently become trapped at the electric-force barrier within the microchannel, leading to the continuous concentration effect. ICP-based ET is insensitive to contamination and PCR inhibitors, is easily integratable with downstream processes, and is reagent-free and low-cost, making it a promising substitute for PCR for NA enrichment in  $\mu$ TAS devices. However, despite the success of ICP-based ET in the concentration of purified analyte in clean buffers, there have been few reports on the application of ICP-based ET with complex biological samples.<sup>40</sup> Cheow et al.<sup>43</sup> demonstrated that the concentration of DNA in donkey serum was possible by ICP-based ET only with at least 10 times dilution (10%) and for only up to 2 min, because the coconcentration of serum proteins caused the rapid back-propagation of the concentration plug toward the inlet. Besides the inability to stably concentrate NAs for long durations in complex biological samples (consequently limiting the enrichment of NAs), the nonselective concentration of NAs, proteins, and other background biomolecules in ICP-based ET poses significant challenges to the purification of NAs for subsequent assays. Hong et al.<sup>44</sup> demonstrated electrophoretic-mobility-based isolation of NAs in ICP-based ET using pneumatic valve systems; this, however, complicates the operations and is difficult to implement in resource-limited settings.

In this paper, we report the direct enrichment and purification of NAs in complex biological samples by pressure-modulated selective electrokinetic trapping (PM-SET), without involving the capture agents and elution chemicals used in SPE, chemical-amplification processes (e.g., PCR), or other complex operations (e.g., valving). We showcase the utility of PM-SET in human serum that contains 60–80 mg/mL total serum protein and perhaps represents one of the most complex backgrounds for molecular detection.<sup>45</sup> Through modulating the hydrostatic pressure applied to the ICP-based ET device, we demonstrate the selective trapping of NAs (of high electrophoretic mobility) while the majority of background proteins (of low electrophoretic mobility) are simultaneously removed, achieving an enrichment factor of  $>4800$  in 15 min for NAs. With the minimal coconcentration

of background proteins, NAs could be stably concentrated with minimal back-propagation. Moreover, we also demonstrate the simultaneous detection of a sequence-specific NA during the enrichment process using a complementary morpholino (MO) probe, achieving picomolar-level detection in 15 min. Unlike conventional surface-hybridization-based NA assays, the MO-probe assay in PM-SET utilizes in-solution hybridization, which does not require surface functionalization, multiple washing steps, or long incubation times. With its ability to directly enrich, purify, and detect NAs in an SPE-free, PCR-free, and surface-hybridization-free manner, we believe PM-SET is promising as a sample-preparation technique that can be fully integrated with existing lab-on-a-chip devices to achieve true micro total-analysis systems for NA detection and as a self-contained biosensor for a variety of NA-detection applications.

## ■ PRINCIPLE OF PM-SET

As shown in Figure 1a, the device consists of a main microchannel, which is split into parallel, narrower channels in the concentration zone. The splitting of a wide channel into multiplexed narrow channels helps stabilize the concentration plugs by suppressing the electrokinetic vortices generated by ICP,<sup>48</sup> which enables the massive scaling up of the channel dimension for high-throughput operations.<sup>47</sup> The cation-selective Nafion membrane (pore diameter: 4 nm)<sup>49</sup> is patterned on the glass slide (bottom of the channels) and bridges the upstream and downstream of the device. The inlet of the device is biased to an electric potential of  $\phi$  ( $>0$ ), and the outlet is grounded (GND). Under this electrical configuration, an electric field,  $E_N$ , is generated across the Nafion membrane as a result of the potential drop from the upstream ends to the downstream end of the membrane. The selective transport of cations through the cation-selective Nafion membrane under  $E_N$  leads to the generation of ion-depletion zones in the microchannels near the Nafion membrane, at the front of which the electric field is significantly amplified. At the same time, a tangential electric field,  $E_T$ , is generated by the potential drop from the inlet ( $\phi$ ) to the outlet (GND), which induces an EOF (velocity:  $v_{EOF}$ ) from the inlet toward the outlet. Negatively charged species enter the microchannels with the EOF but are also subject to a counter-directional electrophoretic force (electrophoretic velocity,  $v_{EP} = \mu E$ , where  $\mu$  is the electrophoretic mobility, and  $E$  is the electric field). In one-dimensional analysis, negatively charged species are trapped near the ion-depletion zone where  $v_{EP}$  becomes as great as  $v_{EOF}$  (net velocity is zero), leading to the continuous-enrichment effect.<sup>46</sup> Because of the high conductivity of the Nafion membrane, the locational

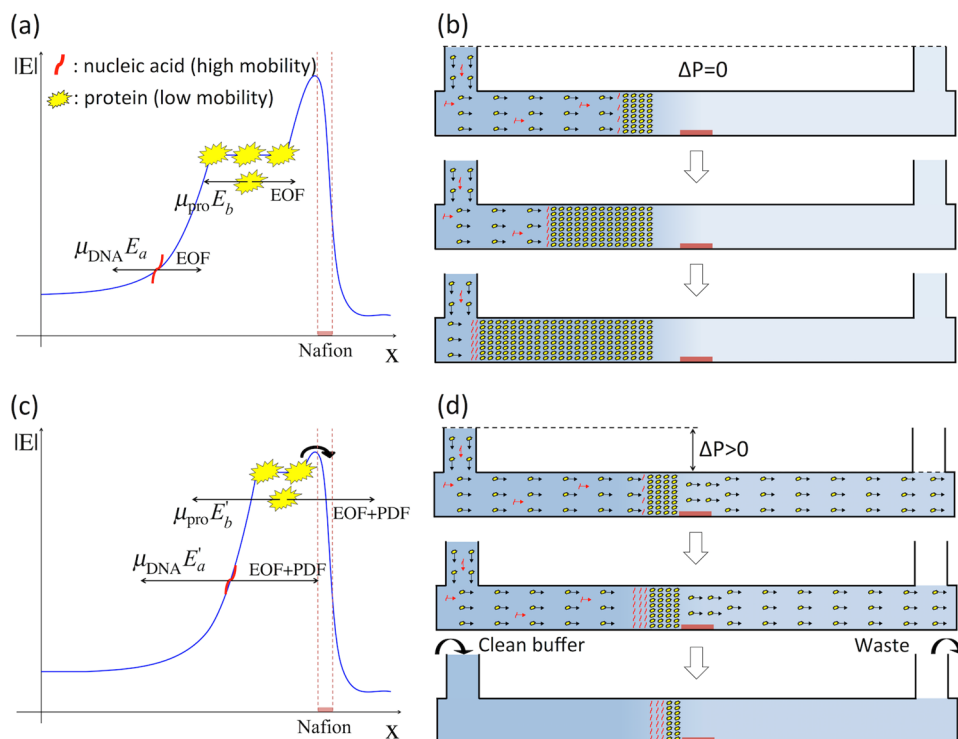


**Figure 2.** Principle of PM-SET. (a) Coconcentration behavior of NAs and proteins at an external hydrostatic pressure of zero. The electrophoretic mobility of NAs is higher than that of proteins, so NAs concentrate farther from the Nafion membrane, where the electric field is weaker, than proteins do. (b) Coconcentration of proteins and NAs causing rapid back-propagation of the NAs. (c) Proteins easily leaking through the electric-force barrier and NAs staying effectively concentrated under external hydrostatic pressure. (d) NAs stably concentrated near the ion-depletion zone and background proteins removed under an external hydrostatic pressure, enabling the simultaneous enrichment and purification of NAs.

dependence of the parallel channels is minimal (i.e., the concentration behaviors in the parallel channels are highly uniform).<sup>47</sup> As shown in Figure 1b, the main channel is 1.6 mm wide and is split into 16 parallel channels 100  $\mu\text{m}$  wide and 10 mm long through evenly bifurcated tree structures. The parallel channels converge into a single channel 1.6 mm wide through structures mirroring the splitting structures. All the channels are 15  $\mu\text{m}$  deep. The Nafion strip is 9 mm from the entrances of the parallel channels (indicated by the blue box and shown in the inset photo in Figure 1b). The parallel channels are sequentially numbered 1–16, as shown in Figure 1b. Figure 1c shows the side view of the device with 1 mL plastic-syringe barrels as the reservoirs.

Figure 2a,b illustrate the concentration behavior in the presence of both NAs and proteins without an external pressure. As previously mentioned, negatively charged biomolecules are trapped where the electric field is  $E = v_{\text{EOF}}/\mu$ . Because the electrophoretic mobility of NAs is much higher than that of proteins ( $\mu_{\text{DNA}} \gg \mu_{\text{pro}}$ ), proteins are concentrated closer to the Nafion membrane, where the electric field is stronger (Figure 2a).<sup>46,50</sup> Under high voltages, as the concentration proceeds, the focused biomolecules (negatively charged) displace the local anions because of the electroneutrality condition until the local anion concentration becomes close to zero, at which point the maximum local concentration of the focused biomolecules is reached, namely, the electroneutrality limit.<sup>51</sup> Because of the high concentration of proteins in human serum (60–80 mg/mL), the proteins instantly reach the electroneutrality limit, after which the concentration of proteins could only proceed by expansion of the protein concentration plug upstream (Figure 2b).

Consequently, NAs are rapidly driven back toward the inlet reservoir to make room for the expanding concentration plug of proteins. Because of the limited length of the channels, NAs could only be concentrated for a short time ( $< 2$  min in the current device in  $1\times$  PBS with 10 mg/mL BSA under 100 V) before reaching the reservoir, resulting in poor enrichment performance. More importantly, the coconcentration of background proteins necessitates the purification of NAs with additional steps, which would otherwise significantly compromise the sensitivity and specificity of downstream assays. Additionally, the inability to stably localize the concentration plug in a specific region of the channels, such as functionalized affinity-capture surfaces, makes it difficult to couple ICP-based ET with conventional surface-hybridization-based assays.

To address the aforementioned challenges in enriching and purifying NAs in complex biological samples, we introduce an additional pressure-driven flow (PDF) into the system, as illustrated in Figure 2c,d. With an external pressure applied to the device, the fluid flow in the microchannels is the superposition of the EOF and PDF. In one-dimensional analysis, negatively charged biomolecules are trapped at the location where  $E = (v_{\text{EOF}} + \bar{v}_{\text{PDF}})/\mu$ , in which  $\bar{v}_{\text{PDF}}$  is the cross-sectional average velocity of the PDF. With the addition of the PDF, biomolecules of the same electrophoretic mobility are concentrated closer to the Nafion membrane, where the electric field is stronger. As shown in Figure 2c, with the pressure appropriately modulated, one could concentrate the proteins in the vicinity of the peak of the electric-force barrier. In this scenario, the concentrated proteins could overcome the electric-force barrier easily by diffusion. As a result, the



concentration of proteins quickly reaches the steady state, at which the influx of proteins is offset by the leakage of proteins across the electric-force barrier. As shown in Figure 2d, in PM-SET, NAs are stably continuously trapped without back-propagation, whereas proteins are continuously leaked and removed from the concentration plug. The hydrostatic pressure is maintained constant by the replenishing of sample or buffer into the inlet and removal of waste from the outlet periodically. Finally, the sample in the inlet is replaced with clean buffer. Afterward, the NAs remain concentrated, whereas the residual proteins in the upstream channel gradually leaked downstream, thereby realizing both the enrichment and purification of NAs. It is noted that, in practice, when we modulated the pressure such that proteins completely overcame the electric-force barrier, there would be strong leakage of NAs across the barrier, or even failure of NA concentration, because of the limited separation resolution between proteins and NAs in the device. Therefore, to ensure the efficient enrichment of NAs, we still have the proteins weakly concentrated in our implementation of PM-SET, as previously described.

## ■ EXPERIMENTAL SECTION

**Reagents and Chemicals.** Phosphate-buffered saline (PBS, 20×) and distilled water were purchased from Thermo Fisher Scientific (Waltham, MA). Solutions of 0.1× PBS, 1× PBS, 2.5× PBS and 5× PBS were prepared by diluting 20× PBS with distilled water to the desired concentrations. Bovine serum albumin (BSA) was purchased from Sigma-Aldrich (St. Louis, MO). Solutions of 100 mg/mL BSA in 0.1× PBS, 1× PBS, 2.5× PBS, and 5× PBS were prepared by dissolving 100 mg BSA in 1 mL PBS buffers of the corresponding concentrations. Human serum was purchased from MilliporeSigma (Burlington, MA). Human serum samples (native ionic strength: ~1× PBS) in 2.5× PBS and 5× PBS were prepared by spiking 0.086 × volume and 0.267 × volume of 20× PBS into 1 × volume of native human serum, respectively. Nafion resin (20 wt % solution in lower aliphatic alcohol/H<sub>2</sub>O mix) was purchased from Sigma-Aldrich (St. Louis, MO). Single-stranded DNAs (ssDNAs) were synthesized and fluorescently labeled by Integrated DNA Technologies (Coralville, IA). A 22 base ssDNA (5'-GTA GGC GAA CCC TGC CCA GGT C-3') with the 3' end labeled with Alexa Fluor 647 was used for the demonstration of NA enrichment. In the DNA-detection experiment, the target DNA was an unlabeled 67 base ssDNA (fragment of the *Mycobacterium tuberculosis* IS6110 gene) with a sequence of 5'- ACC AGC ACC TAA CCG GCT GTG GGT AGC AGA CCT CAC CTA TGT GTC GAC CTG GGC AGG GTT CGC CTA C-3'.<sup>52</sup> The probe for DNA detection was a complementary 22 base MO oligo (5'-GTA GGC GAA CCC TGC CCA GGT C-3') labeled with fluorescein at the 3' end (Gene Tools, LLC, Philomath, OR). BODIPY FL fluorescence dye was purchased from Life Technologies (Carlsbad, CA). Tygon non-DEHP microbore tubing (inner diameter: 0.020 in., outer diameter: 0.060 in.) was purchased from Cole-Parmer (Vernon Hills, IL). A plastic syringe (1 mL) was purchased from Becton, Dickinson and Company (Franklin Lakes, NJ). Ag/AgCl electrodes (diameter: 0.008 in.) were purchased from A-M Systems (Sequim, WA).

**Device Fabrication.** The microchannels were fabricated using polydimethylsiloxane (PDMS; Sylgard 184, Dow Corning Inc., Midland, MI). First, the desired design was

patterned on a silicon wafer using SU-8 photoresist (MicroChem, Westborough, MA) to obtain the master mold, which was subsequently treated with trichlorosilane (Sigma-Aldrich, St. Louis, MO) in a vacuum desiccator overnight to prevent adhesion to PDMS. Next, PDMS was poured onto the master mold. After being cured in an oven at 65 °C for 3 h, the PDMS was peeled off from the master. Access holes of 2 mm in diameter were punched in the PDMS at the inlet and outlet. The Nafion strip was patterned on a glass slide by the microflow-patterning technique using microchannels of 400 μm wide and 50 μm deep and a final thickness of 1.5–1.8 μm.<sup>53</sup> The PDMS chip was irreversibly bonded to the Nafion-patterned glass slide by plasma bonding using the Femto Science Covance Plasma Cleaner (Hwaseong-Si, Gyeonggi-Do, Korea).

**Microfluidic Experiments.** The hydrostatic pressure ( $\Delta P$ ) was determined by the height differences ( $\Delta H$ ) between the liquid levels in the inlet and outlet, which was controlled by the volume differences ( $\Delta V$ ) between the samples loaded into the reservoirs ( $\Delta P = 4\rho g\Delta V/\pi D^2$ , where  $\rho$  is the density of water,  $g$  is the gravitational acceleration, and  $D = 4.78$  mm is the diameter of the syringe barrels). In this work, hydrostatic pressures of 70, 100, 120, and 200 Pa were generated by volume differences of 126, 180, 216, and 360 μL between the inlet and outlet, respectively. For applications where the sample volumes are small (e.g., < 100 μL), an alternative packaging scheme of the device is provided in Section 1 of the SI that allows for the control of the hydrostatic pressure regardless of the sample volume (by adjusting the height of the tubing connected to the outlet).

For the demonstration of NA enrichment by PM-SET, the fluorescently labeled DNA was spiked into BSA-rich buffers and human-serum samples to a final concentration of 1 nM. In the DNA-detection experiment, the MO probe and target DNA were spiked into human serum in 5× PBS to a final MO-probe concentration of 1 nM and final target-DNA concentrations of 1 pM to 100 nM. The MO–DNA mixtures in serum were incubated for 10 min on a vortex mixer before being loaded into the chip.

Before the experiments, the microchannels were passivated with 1% BSA in 1× PBS for 10 min and flushed with 1× PBS afterward. Ag/AgCl electrodes (diameter: 0.008 in.) were inserted into the reservoirs and connected to a DC power supply (Stanford Research Systems, Sunnyvale, CA). In all the experiments, 100 V was applied. The washing step in PM-SET was performed as follows: first, the sample was pipetted out of the inlet; immediately afterward, buffer solution of the same ionic strength and volume was pipetted into the inlet; finally, the device ran for 3 min, after which the concentrated NA could be used for potential subsequent assays. The voltage was kept on during the washing. The concentration plugs would be flushed toward the inlet by the reversed hydrostatic pressure when the sample was pipetted out of the inlet, but they would flow back and be restored near the Nafion a few seconds after the buffer solution was pipetted into the inlet.

Fluorescence images were acquired using an inverted fluorescence microscope (IX71, Olympus, Tokyo, Japan) and a CCD camera (Sensicam qe, Cooke Corporation, Romulus, MI). The exposure time is 100 ms unless otherwise specified. A mechanical shutter was used to reduce the photobleaching effect, which was synchronized with the CCD camera by the open-source software Micromanager.

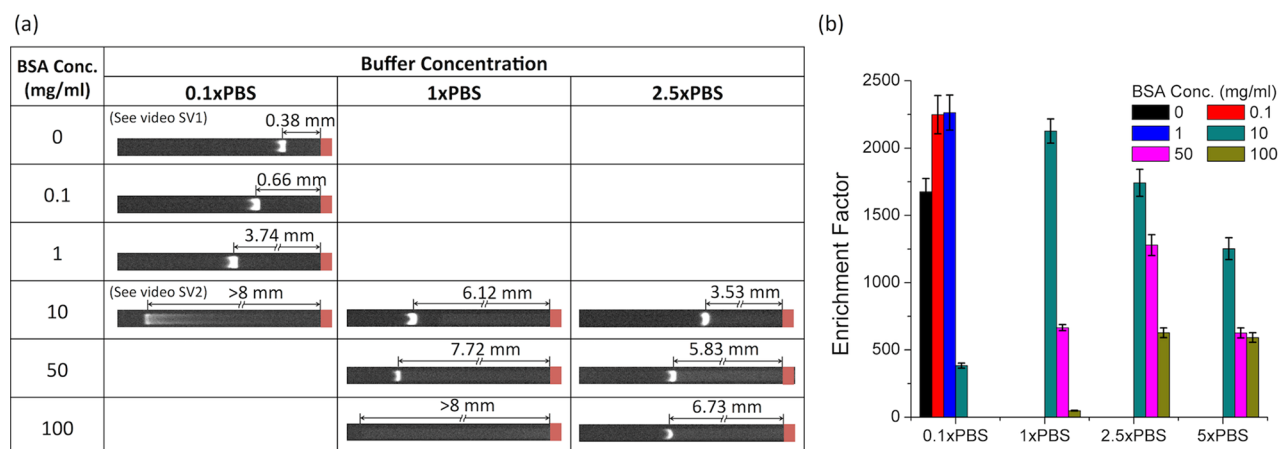


**Figure 3.** Optimization of ionic strength. (a) DNA concentration behaviors at different ionic strengths and BSA concentrations without external pressures in the ninth channel. The dispersion of the DNA concentration plugs at high concentrations of BSA was mitigated by high ionic strengths. The experiments were terminated after 5 min or when the concentration plugs back-propagated beyond the entrances of the parallel channels, whichever happened first. (b) Enrichment factors achieved at different ionic strengths and BSA concentrations at the end of the experiments.

**Data Processing.** The data-processing procedure is described in detail in Section 2 of the SI. Briefly, raw fluorescence micrographs were opened in ImageJ, in which the fluorescence profiles of the channels were measured. On the basis of the fluorescence profiles, the peak fluorescence intensities and the distances between the peaks and Nafion membrane in the channels were extracted in Excel 2010 for Mac. Because of the limited field of view of the fluorescence microscope, we could image no more than 13 channels in our time-lapse imaging. Because the concentration behaviors were highly uniform among the 16 channels,<sup>47</sup> we used data from channels 9–16 (the lower half) to represent the performance of a device (discussed in Section 2 of the SI). Each experimental condition was tested three times using three different devices. We used the grand mean (mean of all  $3 \times 8$  points) and the total standard deviation (of all  $3 \times 8$  points) for each data point and the corresponding error bar, respectively (discussed in Section 2 of the SI).

## RESULTS AND DISCUSSION

**Optimization of Ionic Strength.** We first explored the experimental conditions using BSA in PBS to simulate human serum. Figure 3a shows the concentration plugs of the Alexa Fluor 647 labeled ssDNA under different conditions (different ionic strengths and BSA concentrations). The hydrostatic pressure was zero for all cases. The experiments were terminated when the concentration plug back-propagated beyond the entrances of the parallel channels or after 5 min, whichever happened first. In 0.1× PBS, as we increased the BSA concentration from 0 to 10 mg/mL, the DNA concentration plug significantly back-propagated because of the coconcentration of BSA. More importantly, there was strong dispersion of the DNA concentration plug (forming long tails, see Supplementary Videos SV1 and SV2) at 10 mg/mL BSA, causing significant loss of the DNA. We speculate that this was caused by the nonspecific binding between the highly negatively charged backbone of DNA and positive amino acid residues of BSA at low ionic strengths.<sup>54</sup> As we increased the ionic strength from 0.1× PBS to 1× PBS, dispersion was significantly reduced even with 10 mg/mL BSA. We speculate that this may have benefitted from the effective screening of the surface charges of DNA and BSA at high ion

concentrations. In the meantime, from the perspective of the Kohlrausch regulating function in electrophoresis,<sup>55</sup> more NAs can be concentrated and into narrower zones as the ion concentration increases, which contributes to the less dispersion at high ion concentrations. On the basis of this scheme, we found that DNA with background BSA concentrations of 50–100 mg/mL could be concentrated with significantly reduced dispersion in 2.5× PBS.

On the basis of the fitted linear relationship between the fluorescence intensity and DNA concentration (see Section 3 of the SI), the maximum DNA concentration in a concentration plug ( $c_{\max}$ ) can be calculated by its peak fluorescence intensity. The enrichment factor of a concentration plug is defined as the ratio of the maximum DNA concentration to the initial DNA concentration ( $c_0$ , which is 1 nM in this work), or  $c_{\max}/c_0$ . Figure 3b shows the enrichment factor achieved at the end of the experiments under different conditions. An enrichment factor of  $\sim 2200$  was achieved in 5 min in 0.1× PBS, owing to the high velocity ( $\sim 1$  mm/s, see Section 4 of the SI) of the nonequilibrium EOF generated in this device, which is  $\sim 10$  times faster than conventional electroosmosis.<sup>38</sup> With the increment of the BSA concentrations, the enrichment factor of DNA decreased because of the loss caused by nonspecific binding to BSA. With background BSA concentrations of 50–100 mg/mL, enrichment factors of 500–1500 could be achieved in 2.5× PBS and 5× PBS in 5 min. Lastly, the electric currents of the device in high-ion-concentration buffers were significantly increased but still stable over time (see Section 5 of the SI), indicating that the device could be operated in high ion concentrations.

**Enrichment and Purification of NAs in BSA-Rich Samples by PM-SET.** Using Alexa Fluor 647 labeled ssDNA with a background BSA concentration of 50 mg/mL in 2.5× PBS, we investigated the feasibility of PM-SET for the selective enrichment of NAs. The strong intrinsic fluorescence from 50 mg/mL BSA at an excitation wavelength of  $\sim 488$  nm enabled us to directly image BSA in the device without fluorescence labeling. Figure 4a shows the initial state of the device ( $\varphi = 0$  V). BSA concentration was uniform on the left (upstream) and right (downstream) sides of the Nafion membrane. DNA was not observable at its initial concentration (1 nM). When the hydrostatic pressure was zero (Figure 4b)



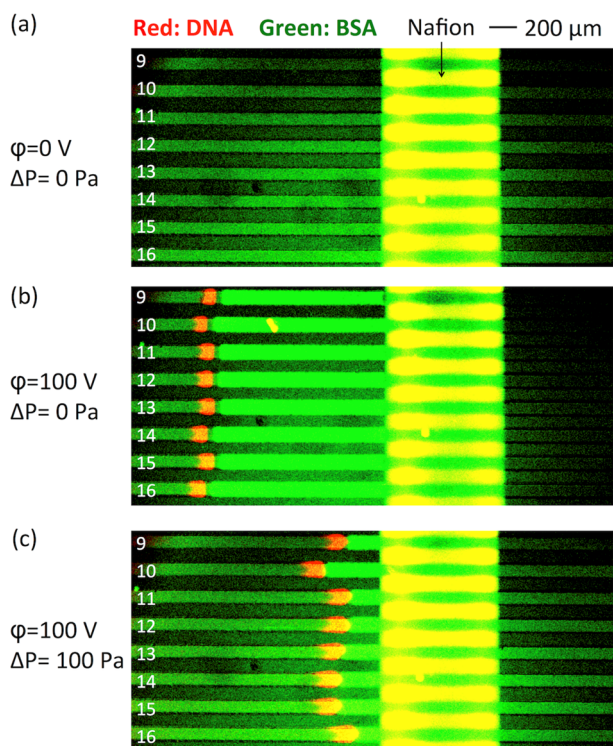


**Figure 4.** Comparison of DNA and BSA concentration behaviors with and without hydrostatic pressure. Fluorescently labeled DNA was imaged at an excitation wavelength of  $\sim 647$  nm. The intrinsic fluorescence of BSA was imaged at an excitation wavelength of  $\sim 488$  nm. The exposure time was 1000 ms. (a) Initial state of the device ( $\phi = 0$  V). The BSA concentration was uniform on the left (upstream) and right (downstream) sides of the channels. DNA (1 nM) was not observable. (b) DNA and BSA coconcentrated near the Nafion at a hydrostatic pressure of zero, resulting in the depletion of BSA downstream. The image was captured at  $t = 30$  s. (c) DNA still effectively concentrated under 100 Pa, with significant leakage of BSA downstream indicated by the fact that the BSA fluorescence downstream was as strong as that upstream. The image was captured at  $t = 30$  s.

after the voltage was on for 30 s, both the DNA and BSA were trapped and concentrated at the upstream side of the Nafion membrane. Consequently, BSA was depleted at the downstream side, as indicated by the vanishing of fluorescence at the downstream side. On the other hand, as shown in Figure 4c, under an appropriate hydrostatic pressure (100 Pa in this case), although DNA was still effectively concentrated, BSA was only weakly concentrated. The expansion of the BSA concentration plugs under 100 Pa was much shorter than that under 0 Pa. The fluorescence intensities of BSA at the upstream and downstream sides were nearly the same, indicating the strong leakage of BSA across the electric-force barrier. Therefore, DNA could be selectively concentrated by PM-SET.

We next studied the temporal behavior of PM-SET. As shown in Figure 5a and Supplementary Video SV3, without external pressure, both DNA and BSA were concentrated, causing rapid back-propagation of the DNA concentration plug. In contrast, under 100 Pa (Figure 5a and Supplementary Video SV4), because of the leakage of BSA across the electric-force barrier, the concentration of BSA reached the steady state within a few seconds, after which the BSA concentration zone no longer expanded. Meanwhile, DNA was continuously

concentrated adjacent to the BSA concentration zone without back-propagation. After 5 min of concentration, a washing step was performed to further purify the background of the concentrated DNA by replacing the sample in the inlet with  $2.5\times$  PBS. As the device continued to operate, residual BSA in the upstream channel escaped to the downstream channel across the electric-force barrier. As shown in Figure 5a (480 s), the BSA concentration zone also shrank, because the BSA in the concentration zone continuously leaked downstream, but the influx of BSA from upstream gradually vanished after buffer replacement. The concentration behaviors under 70 and 120 Pa are shown in Section 6 of the SI.

As shown in Figure 5b, the selectivity of DNA and BSA concentration was dependent on the magnitude of the pressure applied. Under 70 Pa, the leakage rate of BSA was not sufficient to offset the influx of BSA from upstream, which still allowed the continuous concentration of BSA but with a slower speed compared with that under 0 Pa, as inferred from the propagation distances of the DNA concentration plugs. Under 100 Pa, the leakage rate of BSA matched the influx of BSA from upstream, thereby establishing the steady state of BSA concentration. Further increasing the pressure to 120 Pa would enable the escape of both the DNA and BSA, resulting in the failure to concentrate. The enrichment factor of the DNA increased with the pressure owing to the increased influx of the DNA at higher flow rates (Figure 5c), until the failure to concentrate under too high of pressures. An enrichment factor of  $\sim 2400$  was achieved for the DNA in 5 min under 100 Pa.

**Application of PM-SET to NAs in Human Serum.** We next implemented PM-SET to directly enrich and purify NAs in human serum. Figure 6a shows the concentration behaviors of the fluorescently labeled DNA spiked in human serum under different ionic strengths and hydrostatic pressures. DNA in native serum could barely be concentrated because of the strong nonspecific binding between the DNA and background proteins. In native serum, the serum-protein concentration plugs propagated to the entrances of the parallel channels ( $\sim 8$  mm) in a minute, whereas the NA concentration plugs were not observable. As we increased the ionic strength to  $2.5\times$  PBS, the serum-protein concentration plugs reached the entrances of the parallel channels in  $\sim 75$  s, yet the NA concentration plugs were still not resolved. The dispersion problem was mitigated by the increment of the ionic strength to  $5\times$  PBS, at which point a sharp concentration plug of the DNA was formed. However, the coconcentration of serum proteins caused the rapid back-propagation of the DNA concentration plug, which reached the inlet reservoir in  $\sim 5$  min (Figure 6b). With an external pressure of 100 Pa, the leakage of serum proteins across the electric-force barrier did not fully offset the influx of serum proteins from the inlet, resulting in the slower but nonzero back-propagation of the DNA concentration plug. Under 200 Pa, the concentration of serum proteins reached steady state, whereas the DNA was selectively concentrated with minimal back-propagation ( $\sim 1$  mm from the Nafion membrane). With the optimal condition of  $5\times$  PBS and 200 Pa, an enrichment factor of  $\sim 4800$  was achieved for the spiked DNA in human serum in 15 min (Figure 6c).

**Simultaneous Detection of NAs in Human Serum during Enrichment.** NAs enriched and purified by PM-SET can readily be used for subsequent NA assays. Conventional NA assays are typically based on the hybridization of target NAs with surface-immobilized complementary probes, fol-

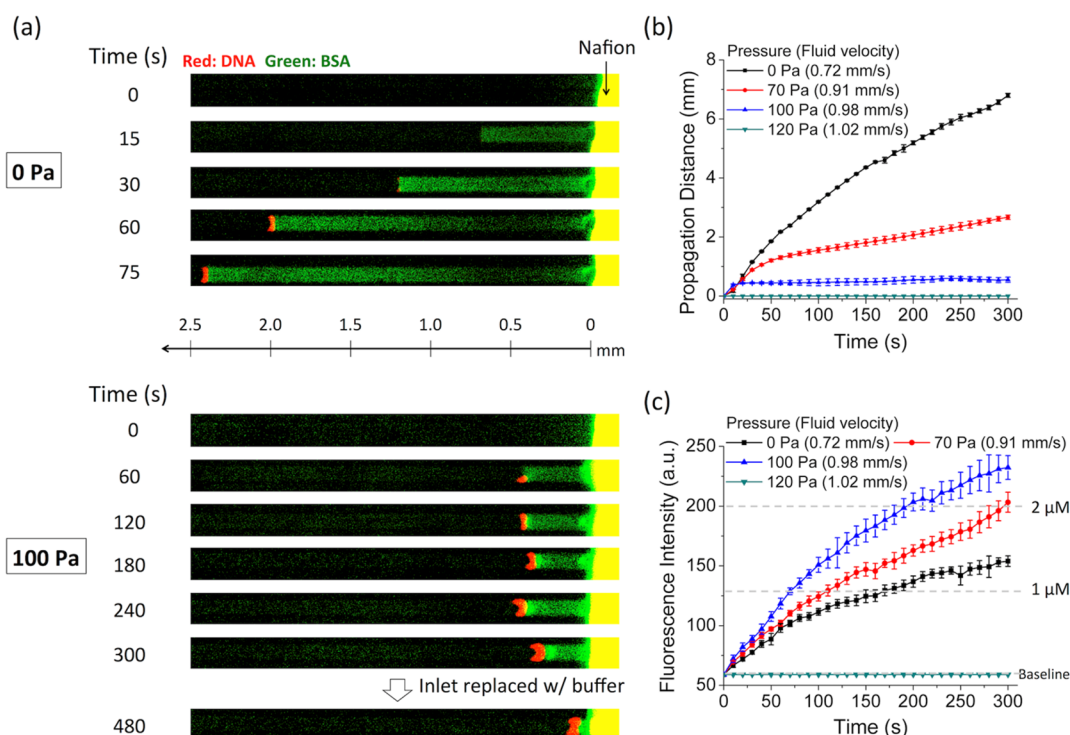


**Figure 5.** Temporal behavior of selective NA enrichment and purification in BSA-rich samples by PM-SET. (a) Overlapped fluorescence images showing the coconcentration of the DNA and BSA under 0 and 100 Pa in the ninth channel. Fluorescently labeled DNA was imaged at an excitation wavelength of  $\sim 647$  nm. The intrinsic fluorescence of BSA was imaged at an excitation wavelength of  $\sim 488$  nm. (b) Back-propagation distances of the DNA concentration plugs under different pressures. The average fluid velocities corresponding to the pressures are labeled in the legend (see Section 4 of the SI). (c) Temporal evolution of the fluorescence intensities of the DNA concentration plugs under different pressures. The reference-DNA concentrations are marked by the dashed lines. The average fluid velocities corresponding to the pressures are labeled in the legend.

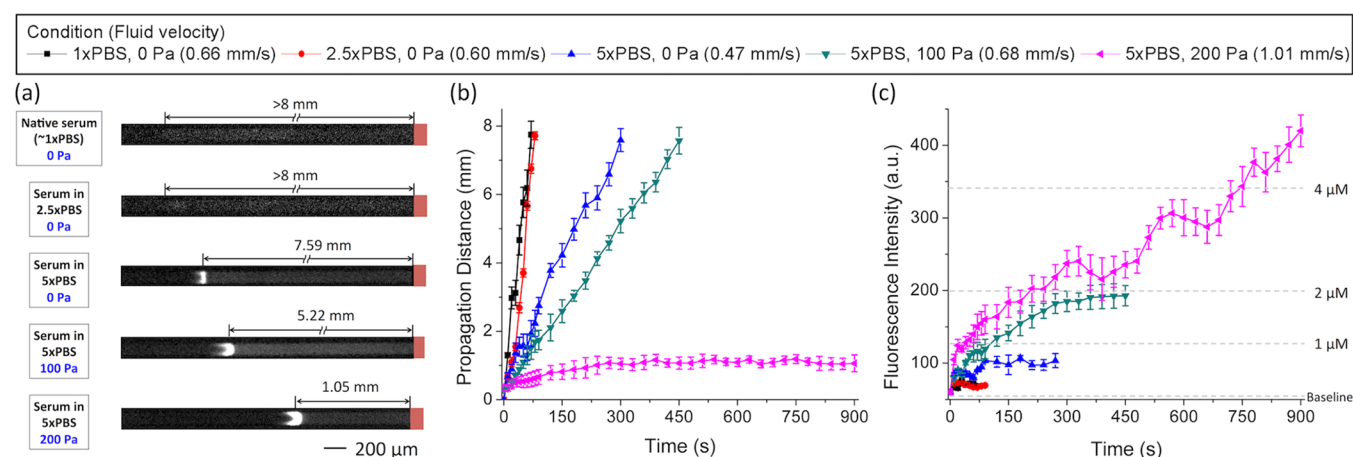


**Figure 6.** Application of PM-SET to NAs in human serum. (a) Optimization of the ionic strength and pressure to realize selective enrichment of the DNA. The fluorescence images represent the ninth channel and were taken at an excitation wavelength of  $\sim 647$  nm. Fluorescence images for native serum and serum in 2.5x PBS were taken when the concentration plugs back-propagated beyond the entrances of the ninth channel. Fluorescence images for serum in 5x PBS were taken after 5 min of concentration. The average fluid velocities corresponding to different conditions are labeled in the legend (see Section 4 of the SI). (b) Back-propagation distances of the NA concentration plugs under different conditions. (c) Temporal evolution of the fluorescence intensities of the DNA concentration plugs under different conditions. Experiments were terminated when the concentration plug back-propagated beyond the entrances of the channels or after 15 min, whichever happened first. The reference-DNA concentrations are marked by the dashed lines.

lowed by electrochemical, optical, and other detection methods.<sup>56–59</sup> In this work, we realized simultaneous detection of a sequence-specific NA in human serum during enrichment using a fluorescently labeled MO probe. As shown in Figure 7a, the MO probe is not charged and hence not subject to an

electrophoretic force in the device, which simply passes the device without being concentrated. However, in the presence of the target DNA, the MO–DNA duplex becomes negatively charged and concentratable. The fluorescence intensity of the concentration plug of the MO–DNA duplex directly reflects



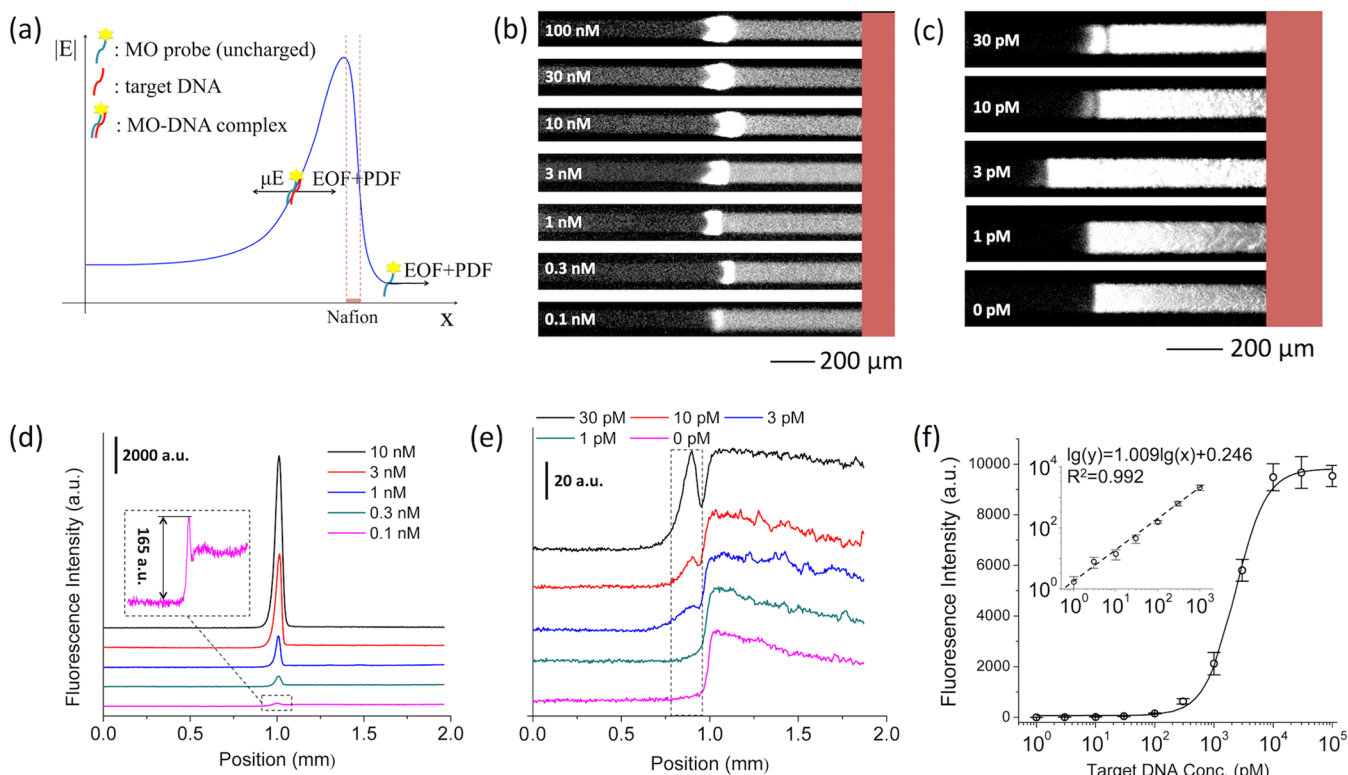


**Figure 7.** Simultaneous detection of a sequence-specific DNA using a complementary MO probe in PM-SET. (a) Schematic of the MO-probe assay in PM-SET. (b) Fluorescence images showing the concentration plugs of the MO–DNA duplex in the ninth channel at 0.1–100 nM target DNA under the 10× objective lens. (c) Fluorescence images showing the concentration plugs of the MO–DNA duplex in the ninth channel at 0–30 pM target DNA under the 20× objective lens. (d) Fluorescence profiles along the ninth channel at 0.1–100 nM target DNA under the 10× objective lens. The peaks of the fluorescence profiles are aligned on the x-axis. The fluorescence profiles are displaced by 1000 au on the y-axis to better visualize individual profiles. The fluorescence profile corresponding to 0.1 nM is magnified in the dashed-line box. (e) Fluorescence profiles along the ninth channel at 0–30 pM target DNA under the 20× objective lens. The peaks corresponding to the MO–DNA duplex are shown in the dashed-line box. The peaks of fluorescence profiles are aligned on the x-axis. The fluorescence profiles are displaced by 20 au on the y-axis to better visualize individual profiles. (f) Dose–response curve of the assay (fitted using the four-parameter logistic function). The inset log–log plot shows the linear relationship at lower concentrations of target DNA.

the concentration of the target DNA. As shown in Figure 7b, the fluorescence intensity of the MO–DNA concentration plug decreased with the concentration of target DNA. An MO–DNA concentration plug below a 100 pM concentration of target DNA was resolved by using the 20× objective lens (Figure 7c). The fluorescence profiles along the channel at 0.1–10 nM and 0–30 pM target DNA were plotted in Figure 7d,e, respectively, which show that peaks corresponding to the MO–DNA duplex are resolved down to 3 pM. The full dynamic range of the assay is shown in Figure 7f, which was fitted using the four-parameter logistic function (see Section 7 of the SI).<sup>60</sup> The inset figure of Figure 7f shows a linear relationship in the log–log plot at low target-DNA concentrations (0–1000 pM), with a minimum concentration of 3 pM detected. In the negative control, we did not observe a concentration plug of MO–DNA duplex.

The MO-probe assay in PM-SET offers a number of advantages over conventional surface-hybridization-based NA assays: (1) The in-solution hybridization significantly shortens the incubation time (10 min in this work) as a result of the much faster kinetics, whereas surface-hybridization-based assays take many hours.<sup>61,62</sup> (2) The MO-probe assay is directly coupled with the enrichment process without the surface-functionalization and multiple washing steps needed in surface-hybridization-based assays. (3) Surface-hybridization-

based assays often suffer from the nonspecific binding of proteins onto the surface, which compromises the sensitivity of the assays. In the MO-probe assay, the nonspecifically bound complexes of the MO probe and serum proteins are not concentratable and hence do not affect the assay. (4) The MO probe has better specificity than conventionally used DNA probes.<sup>63</sup>

## CONCLUSIONS

In this paper, we demonstrate PM-SET for the direct enrichment, purification, and detection of NAs in human serum. NAs were selectively enriched by ~4800 times in 15 min while the background proteins were removed, without the need of the conventionally used SPE and PCR. PM-SET significantly reduces the time, cost, and complexity of sample preparation for NA detection in complex biological samples. Most importantly, PM-SET is based on a simple device structure and a simple operation procedure (DC voltage and hydrostatic pressure), which could be fully integrated with existing lab-on-a-chip NA sensors to achieve true sample-to-answer systems. PM-SET also simultaneously detects sequence-specific NAs in human serum as low as 3 pM in 15 min during the enrichment process, which significantly shortens the detection time and simplifies the operation procedures compared with surface-hybridization-based assays.

With these advantages, we believe that PM-SET could potentially play an enabling role in the development of lab-on-a-chip devices toward point-of-care diagnostics, on-site food and environment monitoring, and a variety of other applications in resource-limited settings. The next step toward the final application of this platform would include a modeling study of PM-SET. The hydrostatic pressure needed to selectively and stably enrich NAs in a sample is affected by its protein concentration, ionic strength, and viscosity, which is currently determined in a case-by-case manner. As sample properties differ, deeper understanding and modeling of PM-SET would help to eliminate the need for sample-by-sample calibration to determine the optimal experimental conditions.

## ■ ASSOCIATED CONTENT

### ■ Supporting Information

The Supporting Information is available free of charge on the ACS Publications website at DOI: 10.1021/acs.analchem.8b02330.

Alternative packaging scheme of the device, data processing, calculation of the enrichment factor, measurement of fluid velocity, stability of the electric current, temporal evolution of the DNA concentration plugs under 70 and 120 Pa, and fitting parameters of the dose–response curve (PDF)

Supplementary Video SV1. Concentration of fluorescently labeled DNA in 0.1× PBS with 0 mg/mL BSA (pressure = 0 Pa). The video is 50× accelerated (MPG) Supplementary Video SV2. Concentration of fluorescently labeled DNA in 0.1× PBS with 10 mg/mL BSA (pressure = 0 Pa). The video is 50× accelerated (MPG) Supplementary Video SV3. Concentration of fluorescently labeled DNA in 2.5× PBS with 50 mg/mL BSA (pressure = 0 Pa). The video is 50× accelerated (MPG) Supplementary Video SV4. Concentration of fluorescently labeled DNA in 2.5× PBS with 50 mg/mL BSA (pressure = 100 Pa). The video is 50× accelerated (MPG)

## ■ AUTHOR INFORMATION

### Corresponding Authors

\*E-mail: lizirui@gmail.com (Z.L.).

\*E-mail: jyhan@mit.edu (J.H.).

### ORCID

Wei Ouyang: 0000-0003-4279-661X

### Notes

The authors declare no competing financial interest.

## ■ ACKNOWLEDGMENTS

This work was supported by the NIH (Grant Numbers U19AI109755 and R01AI117043) and the National Natural Science Foundation of China (Grant Numbers 11372229 and 21576130).

## ■ REFERENCES

- (1) Gootenberg, J. S.; Abudayyeh, O. O.; Lee, J. W.; Essletzbichler, P.; Dy, A. J.; Joung, J.; Verdine, V.; Donghia, N.; Daringer, N. M.; Freije, C. A.; et al. *Science* **2017**, 356, 438–442.
- (2) Baaske, M. D.; Foreman, M. R.; Vollmer, F. *Nat. Nanotechnol.* **2014**, 9, 933.

- (3) Ceuppens, S.; Li, D.; Uyttendaele, M.; Renault, P.; Ross, P.; Ranst, M. V.; Coccolin, L.; Donaghy, J. *Compr. Rev. Food Sci. Food Saf.* **2014**, 13, 551–577.
- (4) Kim, T.-H.; Park, J.; Kim, C.-J.; Cho, Y.-K. *Anal. Chem.* **2014**, 86, 3841–3848.
- (5) Niemcz, A.; Ferguson, T. M.; Boyle, D. S. *Trends Biotechnol.* **2011**, 29, 240–250.
- (6) Easley, C. J.; Karlinsey, J. M.; Bienvenue, J. M.; Legendre, L. A.; Roper, M. G.; Feldman, S. H.; Hughes, M. A.; Hewlett, E. L.; Merkel, T. J.; Ferrance, J. P.; et al. *Proc. Natl. Acad. Sci. U. S. A.* **2006**, 103, 19272–19277.
- (7) Chin, C. D.; Linder, V.; Sia, S. K. *Lab Chip* **2007**, 7, 41–57.
- (8) Reyes, D. R.; Iossifidis, D.; Auroux, P.-A.; Manz, A. *Anal. Chem.* **2002**, 74, 2623–2636.
- (9) Chen, L.; Manz, A.; Day, P. J. R. *Lab Chip* **2007**, 7, 1413–1423.
- (10) Auroux, P. A.; Koc, Y.; deMello, A.; Manz, A.; Day, P. J. R. *Lab Chip* **2004**, 4, 534–546.
- (11) Yager, P.; Edwards, T.; Fu, E.; Helton, K.; Nelson, K.; Tam, M. R.; Weigl, B. H. *Nature* **2006**, 442, 412.
- (12) Whitesides, G. M. *Nature* **2006**, 442, 368.
- (13) Mariella, R. *Biomed. Microdevices* **2008**, 10, 777.
- (14) Lim, Y. C.; Kouzani, A. Z.; Duan, W. *Microsyst. Technol.* **2010**, 16, 1995–2015.
- (15) Persat, A.; Marshall, L. A.; Santiago, J. G. *Anal. Chem.* **2009**, 81, 9507–9511.
- (16) Choi, S.; Goryll, M.; Sin, L. Y. M.; Wong, P. K.; Chae, J. *Microfluid. Nanofluid.* **2011**, 10, 231–247.
- (17) Sin, M. L. Y.; Gao, J.; Liao, J. C.; Wong, P. K. *J. Biol. Eng.* **2011**, 5, 6.
- (18) Byrnes, S.; Thiessen, G.; Fu, E. *Bioanalysis* **2013**, 5, 2821–2836.
- (19) Ritzi-Lehnert, M. *Expert Rev. Mol. Diagn.* **2012**, 12, 189–206.
- (20) Nezhad, A. S. *Lab Chip* **2014**, 14, 2887–2904.
- (21) Bienvenue, J. M.; Legendre, L. A.; Ferrance, J. P.; Landers, J. P. *Forensic Sci. Int.: Genet.* **2010**, 4, 178–186.
- (22) Hagan, K. A.; Bienvenue, J. M.; Moskaluk, C. A.; Landers, J. P. *Anal. Chem.* **2008**, 80, 8453–8460.
- (23) Huang, S.; Do, J.; Mahalanabis, M.; Fan, A.; Zhao, L.; Jepeal, L.; Singh, S. K.; Klapperich, C. M. *PLoS One* **2013**, 8, e60059.
- (24) Wu, Q.; Jin, W.; Zhou, C.; Han, S.; Yang, W.; Zhu, Q.; Jin, Q.; Mu, Y. *Anal. Chem.* **2011**, 83, 3336–3342.
- (25) Shaw, K. J.; Joyce, D. A.; Docker, P. T.; Dyer, C. E.; Greenway, G. M.; Greenman, J.; Haswell, S. J. *Lab Chip* **2011**, 11, 443–448.
- (26) Duarte, G. R. M.; Price, C. W.; Augustine, B. H.; Carrilho, E.; Landers, J. P. *Anal. Chem.* **2011**, 83, 5182–5189.
- (27) Liu, D.; Liang, G.; Zhang, Q.; Chen, B. *Anal. Chem.* **2013**, 85, 4698–4704.
- (28) Hagan, K. A.; Meier, W. L.; Ferrance, J. P.; Landers, J. P. *Anal. Chem.* **2009**, 81, 5249–5256.
- (29) Cao, W.; Easley, C. J.; Ferrance, J. P.; Landers, J. P. *Anal. Chem.* **2006**, 78, 7222–7228.
- (30) Oblath, E. A.; Henley, W. H.; Alarie, J. P.; Ramsey, J. M. *Lab Chip* **2013**, 13, 1325–1332.
- (31) Reinholdt, S. J.; Baeumner, A. J. *Angew. Chem., Int. Ed.* **2014**, 53, 13988–14001.
- (32) Zhang, C.; Xing, D. *Nucleic Acids Res.* **2007**, 35, 4223–4237.
- (33) Chang, C.-M.; Chang, W.-H.; Wang, C.-H.; Wang, J.-H.; Mai, J. D.; Lee, G.-B. *Lab Chip* **2013**, 13, 1225–1242.
- (34) Asiello, P. J.; Baeumner, A. J. *Lab Chip* **2011**, 11, 1420–1430.
- (35) Ahrberg, C. D.; Manz, A.; Chung, B. G. *Lab Chip* **2016**, 16, 3866–3884.
- (36) Ahmad, F.; Hashsham, S. A. *Anal. Chim. Acta* **2012**, 733, 1–15.
- (37) Craw, P.; Balachandran, W. *Lab Chip* **2012**, 12, 2469–2486.
- (38) Wang, Y.-C.; Stevens, A. L.; Han, J. *Anal. Chem.* **2005**, 77, 4293–4299.
- (39) Kim, S. J.; Song, Y.-A.; Han, J. *Chem. Soc. Rev.* **2010**, 39, 912–922.
- (40) Fu, L. M.; Hou, H. H.; Chiu, P. H.; Yang, R. J. *Electrophoresis* **2018**, 39, 289–310.

- (41) Li, M.; Anand, R. K. *Analyst* **2016**, *141*, 3496–3510.
- (42) Ouyang, W.; Han, J.; Wang, W. *Lab Chip* **2017**, *17*, 3006–3025.
- (43) Cheow, L. F.; Han, J. *Anal. Chem.* **2011**, *83*, 7086–7093.
- (44) Hong, S. A.; Kim, Y.-J.; Kim, S. J.; Yang, S. *Biosens. Bioelectron.* **2018**, *107*, 103–110.
- (45) Walker, H. K.; Hall, W. D.; Hurst, J. W. *Clinical Methods: The History, Physical, and Laboratory Examinations*; Butterworth Publishers, 1990.
- (46) Gong, L.; Ouyang, W.; Li, Z.; Han, J. *AIP Adv.* **2017**, *7*, 125020.
- (47) Ko, S. H.; Kim, S. J.; Cheow, L. F.; Li, L. D.; Kang, K. H.; Han, J. *Lab Chip* **2011**, *11*, 1351–1358.
- (48) Kim, K.; Kim, W.; Lee, H.; Kim, S. J. *Nanoscale* **2017**, *9*, 3466–3475.
- (49) Mauritz, K. A.; Moore, R. B. *Chem. Rev.* **2004**, *104*, 4535–4586.
- (50) Ouyang, W.; Ko, S. H.; Wu, D.; Wang, A. Y.; Barone, P. W.; Hancock, W. S.; Han, J. *Anal. Chem.* **2016**, *88*, 9669–9677.
- (51) Ouyang, W.; Ye, X.; Li, Z.; Han, J. *Nanoscale* **2018**, *10*, 15187–15194.
- (52) Cannas, A.; Goletti, D.; Girardi, E.; Chiacchio, T.; Calvo, L.; Cuzzi, G.; Piacentini, M.; Melkonyan, H.; Umansky, S. R.; Lauria, F. N.; et al. *Int. J. Tuberc. Lung Dis.* **2008**, *12*, 146–151.
- (53) Ko, S. H.; Song, Y.-A.; Kim, S. J.; Kim, M.; Han, J.; Kang, K. H. *Lab Chip* **2012**, *12*, 4472–4482.
- (54) Jantz, D.; Berg, J. M. *Biophys. J.* **2010**, *98*, 852–860.
- (55) Hruška, V.; Gaš, B. *Electrophoresis* **2007**, *28*, 3–14.
- (56) Huang, C.-J.; Lin, Z.-E.; Yang, Y.-S.; Chan, H. W.-H.; Chen, W.-Y. *Biosens. Bioelectron.* **2018**, *99*, 170–175.
- (57) Diao, W.; Tang, M.; Ding, S.; Li, X.; Cheng, W.; Mo, F.; Yan, X.; Ma, H.; Yan, Y. *Biosens. Bioelectron.* **2018**, *100*, 228–234.
- (58) Rashid, J. I. A.; Yusof, N. A. *Sensing and Bio-Sensing Research* **2017**, *16*, 19–31.
- (59) Irving, D.; Gong, P.; Levicky, R. *J. Phys. Chem. B* **2010**, *114*, 7631–7640.
- (60) Wild, D. *The immunoassay handbook: theory and applications of ligand binding, ELISA and related techniques*; Newnes, 2013.
- (61) Martins, D.; Wei, X.; Levicky, R.; Song, Y.-A. *Anal. Chem.* **2016**, *88*, 3539–3547.
- (62) Martins, D.; Levicky, R.; Song, Y.-A. *Biosens. Bioelectron.* **2015**, *72*, 87–94.
- (63) Summerton, J. E. *Curr. Top. Med. Chem.* **2007**, *7*, 651–660.